BEAM NORMAL SINGLE SPIN ASYMMETRY IN FORWARD ANGLE INELASTIC ELECTRON-PROTON SCATTERING USING THE Q^P_{WEAK} APPARATUS

A Dissertation

By

NURUZZAMAN

Submitted to the Graduate College of Hampton University in
partial fulfillment of the requirements for the degree of

DOCTOR OF PHILOSOPHY

April 2014

TABLE OF CONTENTS

Section Page

1 Experimental Setup 1

1.1 Q-weak Kinematics 1

1.2 TJNAF Overview 2

1.2.1 Polarized Source and Helicity Reversal 3

1.3 Accelerator 6

1.3.1 LINAC 6

1.4 Beamline 6

1.5 Beam Monitoring 7

1.5.1 Beam Position Monitor 7

1.5.2 Superharp 9

1.5.3 Beam Current Monitor 9

1.5.4 Beam Energy 9

1.5.4.1 Absolute Beam Energy 10

1.5.4.2 Energy Asymmetry 10

1.5.5 Beam Modulation 11

1.5.6 Halo Monitors 11

1.6 Polarimetry 11

1.6.1 Moller Polarimetry 13

1.6.2 Compton Polarimetry 14

1.7 Targets 14

1.7.1 Liquid Hydrogen Target 14

1.7.1.1 Raster 16

1.7.2 Solid Target 16

1.8 Collimators and Shielding 17

1.9 Q-weak Toroidal Magnetic Spectrometer: QTor 17

1.9.1 Hall Probe 18

1.10 Detector System 19

1.10.1 Main Čerenkov Detectors 19

Section Page

1.10.1.1 Low Noise Electronics 21

1.10.1.2 Focal Plane Scanner 21

1.10.2 Luminosity Monitors 21

1.11 Tracking Detector System 22

1.12 Data Acquisition 22

BIBLIOGRAPHY **24**

LIST OF TABLES

Table Page

1.1 Proposed error budget of the Q-weak experiment. 1

1.2 Basic parameters and typical operating conditions of the Q-weak experiment 3

LIST OF FIGURES

Figure		Page
1.1	Sketch of the elastic electron-proton scattering process.	2
1.2	Jefferson Lab and its beamline schematic.	4
1.3	Schematic showing the process of producing circularly polarized light.	5
1.4	Beam position and current monitors.	7
1.5	Schematic diagram of the Q-weak apparatus.	12
1.6	Layout of the Hall C Moller polarimeter.	12
1.7	Schematic of the Hall C Compton polarimeter.	13
1.8	Q-weak target system.	15
1.9	Raster scan.	16
1.10	Q-weak torodial magnetic spectrometer (QTor).	18
1.11	QTor controls and hall probe.	19
1.12	Q-weak main Čerenkov detector system.	20
1.13	ADC	20
1.14	Luminosity monitors.	22

SECTION 1

EXPERIMENTAL SETUP

The Q-weak experiment (E08-016) was performed at Thomas Jefferson National Accelerator Facility (TJNAF) [1] in Newport News, Virginia from January 2011 to May 2012 [2–4]. The goal of the Q-weak experiment is to extract the weak charge the of proton by the measuring parity violating (PV) asymmetry in elastic electron-proton scattering at low momentum transfer. The Standard Model (SM) predicts this asymmetry to be -230 parts per billion (ppb) and the Q-weak collaboration proposed to measure this asymmetry with 2.1% statistical uncertainty. The Q-weak experiment ~~was~~ has highly benefited from technologies developed by previous parity violating experiments ~~like~~ such as SAMPLE [5] at the MIT/Bates Linear Accelerator Center, G0 [6] and HAPPEX [7] at JLab. As the Q-weak PV asymmetry and its absolute uncertainty ~~is~~ are an order of magnitude smaller than its predecessors (smallest asymmetry and absolute uncertainty measured in e-p scattering till date), a dedicated design, significant improvement to hardware and software, and additional control of systematic uncertainties were needed to reach the proposed precision goals summarized in Table 1.1.

this seems oddly placed here.

Source of Error	$\frac{\Delta A_{PV}}{A_{PV}}$	$\frac{\Delta Q_W^p}{Q_W^p}$
Statistics	2.1%	3.2%
Hadronic structure	-	1.5%
Beam polarization	1.0%	1.5%
Absolute Q^2	0.5%	1.0%
Backgrounds	0.7%	0.7%
Helicity correlated beam properties	0.5%	0.8%
Total	2.6%	4.2%

Table 1.1 Proposed error budget of the Q-weak experiment [4]. The second and third columns show the relative uncertainty on parity violating asymmetry, and on weak charge of proton respectively.

1.1 Q-weak Kinematics

In ~~a~~ two-body elastic electron-proton scattering, an incident electron with energy E and momentum p scatters from a stationary proton with mass M. The ~~scattered~~ electron ~~traverses~~ scatters with energy E' and momentum p_0 at an angle θ with respect to ~~its initial trajectory~~ incident as shown in Figure 1.1. The

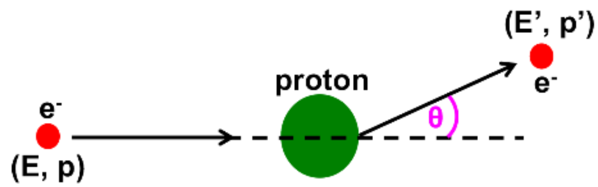

Figure 1.1 Sketch of the elastic electron-proton scattering process.

energy transfer can be expressed as $\gamma = E - E'$ and 3-momentum transfer as $\mathbf{q} = \mathbf{p}$ - $\mathbf{p}'$. Then the four momentum transfer can be defined as

$$Q^2 = -q^2 = -(\nu^2 - \mathbf{q}^2) \geq 0 \tag{1.1.1}$$

Using energy and momentum conservation for two-body scattering, the scattered energy E' and Q^2 can be written as

$$E' = \frac{E}{1 + 2\frac{E}{M}\sin^2\frac{\theta}{2}} \tag{1.1.2}$$

$$Q^2 = \frac{4E^2\sin^2\frac{\theta}{2}}{1 + 2\frac{E}{M}\sin^2\frac{\theta}{2}} \tag{1.1.3}$$

A dedicated tracking system was used to measure the scattering angle θ and Q^2 to improve simulation (more details in Section 1.11). A longitudinally polarized electron beam with energy 1.155 GeV was ~~used as~~ incident ~~beam~~ on a 35 cm long liquid hydrogen target (LH_2), where a 9000A spectrometer selected out the ~~for~~ elastic e-p scattering at l~~ow~~ Q^2 = (0.025 (GeV/c)^2). A summary of the basic parameters and typical operating conditions for the experiment are shown in Table 1.2. The design parameters of the experiment were chosen to minimize the contributions from the anticipated systematic uncertainties shown in Table 1.1.

huh?? We couldn't do it with just simulation. Rather we used simulation to confirm measurement

1.2 TJNAF Overview

Didn't you just use this above? Now you can use TJNAF

The electron accelerator in Thomas Jefferson National Accelerator Facility (TJNAF) or Jefferson Lab (JLab) is known as the Continuous Electron Beam Accelerator Facility (CEBAF) [10], uses superconducting radio frequency (SRF) technology to accelerate polarized electrons up to 6 GeV and is capable of simultaneous beam delivery to all three experimental halls (A, B and C) at different energies, ~~at different~~ beam intensities, and ~~different~~ orientation of beam polarization. The

not just polarized.

Parameter	Value
Incident beam energy	1.155 GeV
Beam polarization	89%
Beam current	180 μA
LH_2 target thickness	34.4 cm
Cryopower	2.5 kW
Production running time	2544 hours
Nominal scattering angle	7.9^o
Scattering angle acceptance	$\pm 3^o$
Acceptance	49% of 2π
Solid angle	$\Delta\Omega$ = 43 msr
Acceptance averaged Q^2	$\langle Q^2 \rangle$ = 0.025 $(\mathrm{GeV/c})^2$
Acceptance averaged physics asymmetry	$\langle A \rangle$ = -234 ppb
Acceptance averaged experimental asymmetry	$\langle A \rangle$ = -200 ppb
Luminosity	2×10^{39} $\mathrm{s^{-1}cm^{-2}}$
Integrated cross section	4.0 μb
Integrated rate	(all sectors) 6.5 GHz (0.81 GHz per sector)
Full Current Production Running	2544 hours

Table 1.2 Basic parameters and typical operating conditions of the Q-weak experiment [4,8,9]

(carried out?)

Q-weak experiment was performed in experimental Hall-C during January 2011 to May 2012, although preparation ~~started~~ began in 2001. In the future, JLab will be upgrade ~~it's~~ its energy from 6 GeV to 12 GeV, and a new experimental hall (Hall-D) will be added [11]. A schematic of ~~the~~ CEBAF is shown in Figure 1.2 (f). The JLab electron beam starts from a polarized source and end in the beam dump at the end station. The longitudinally polarized beam from the source ~~goes~~ starts and travels through a ~~bunch~~ series of spin rotators, and then accelerated by two linear accelerators and ~~enter~~ ends in the experimental Hall-C. Throughout the beamline, quadrupoles and dipoles were used to focus/defocus the beam and beam position, and current monitors were used to track the beam at any given point ~~and time~~ along the accelerator. Inside ~~the~~ Hall-C the beam scatters from the target and the scattered electrons passes through a series of collimators and a toroidal magnet then focuses these scattered electrons into the Čerenkov detector and unscattered beam goes to beam dump. This chapter will discuss various key components of the experimental apparatus in following subsections.

Is this necessary?

I would remove this. It sort of is explained by the next sentence.

Consider re-writting this last pharagraph. It's kind of repetitive from what you already said with only mindly more detail.

1.2.1 Polarized Source and Helicity Reversal

The production of the electron beam starts with the polarized electron source. Circularly polarized light is used to produce polarized electrons from a strained super-lattice Gallium-Arsenide (GaAs) cathode via the photo-electric effect. This cathode is ~~made up~~ composed of several layers of material containing GaAs with varying amounts of phosphorus doping, grown on a substrate. Supperlattice

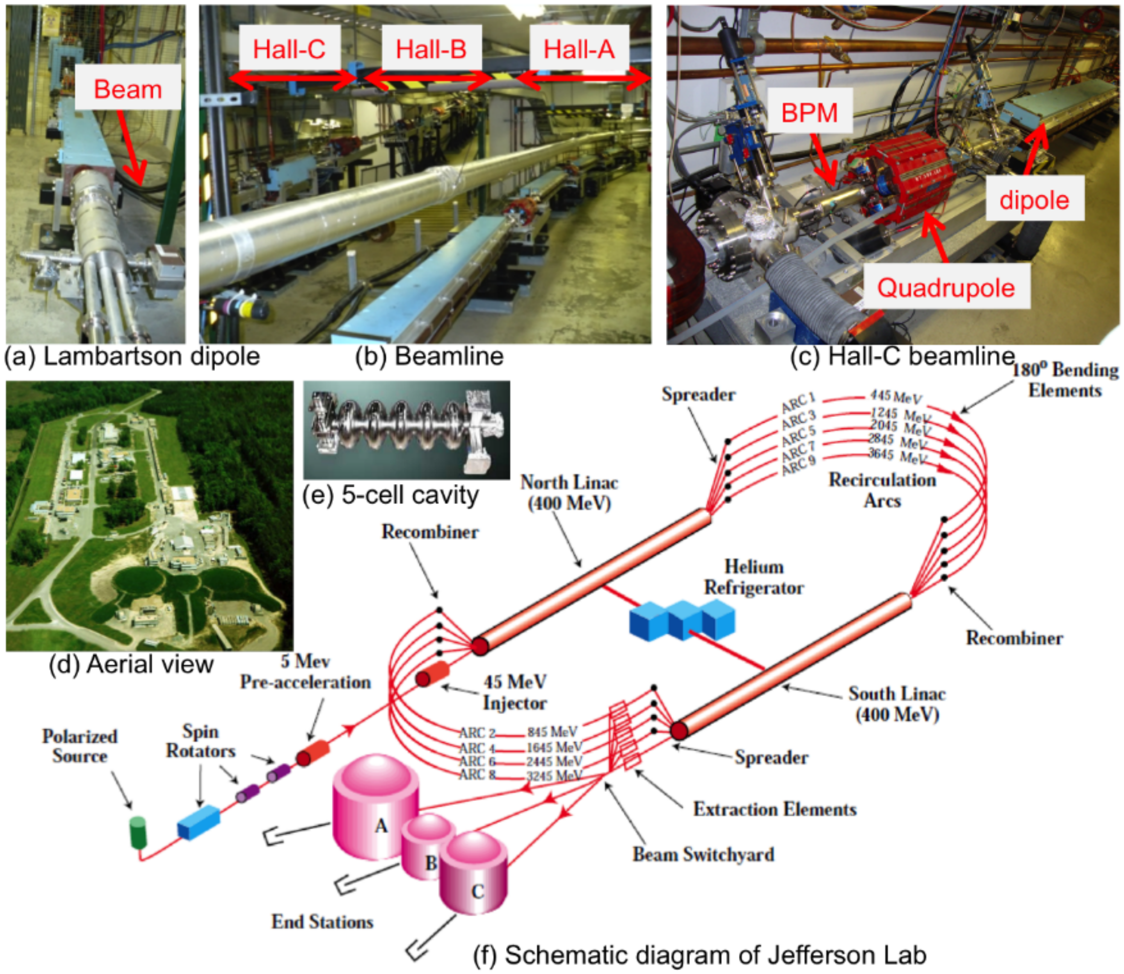

Figure 1.2 Jefferson Lab and its beamline schematic. (a) Lambartson Dipole at BSY region where beam splits for three different experimental halls. (b) Three seperate beamline for three halls. (c) Hall-C beamline before entering in the hall. A typical quadrupole, dipole, and BPM are shown. (d) Aerial view of Jefferson Lab. (e) A JLab made 5-cell accelerating cavity. (f) Schematic diagram of Jefferson Lab. The elliptical region is the electron accelerator. Beam is accelerated by two linear accelerator namely North and South linac in the straight sections. Three existing Halls A, B, C are shown.

structure (alternating layers of GaAs and strained GaAs) increased the quantum efficiency (QE), which is the probability of electron emission per photon [12]. Each experimental hall has a dedicated LASER that emits light at 1560 nm and pulses are 120^o out of phase in order to provide beam delivery in all halls simultaneously. To ensure total linear polarization, the light was passed through linear polarizers (shown in Figure 1.3). An insertable half wave plate (IHWP) was used to flip the relative direction of the linearly polarized light without changing electronic helicity signal, which helps to isolate false asymmetry effects ~~that changes with true electron beam helicity~~. IHWP changes the

has become common word, use laser

kind of confuses the message.

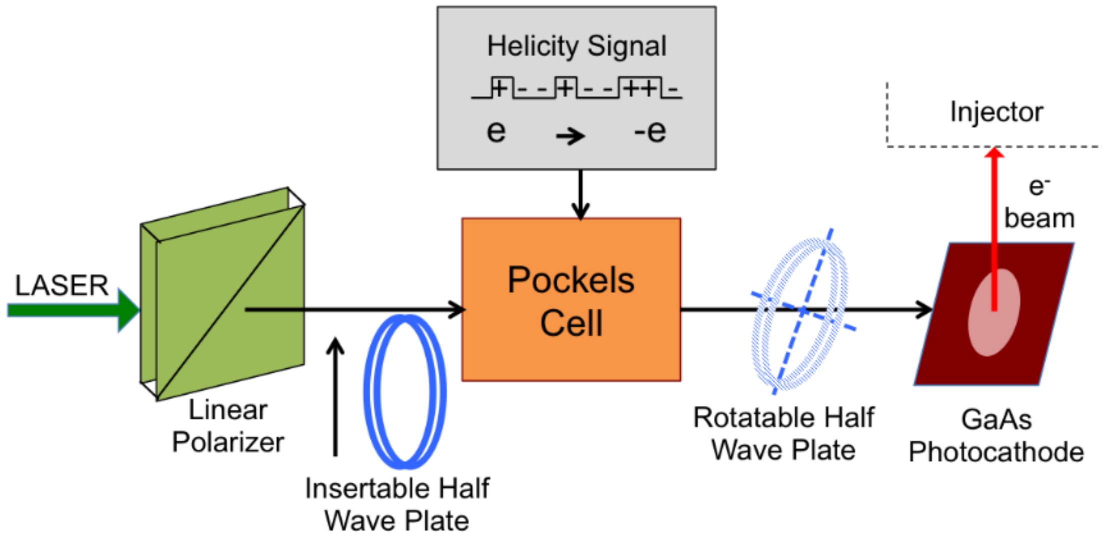

Figure 1.3 Schematic showing the process of producing circularly polarized light. The LASER is circularly polarized before GaAs photocathode using Pockels cell.

spin of the electrons by 180^o, this provided two independent data sets, namely IHWP-IN and IHWP-OUT, that helped remove further helicity correlated beam asymmetries (HCBA). IHWP states were changed at a time interval of eight hours, ~~which is~~ called slugs. A pockel~~s~~ cell was used to convert linearly polarized light to circularly polarized electrons using induced birefringence. Just after the pockel~~s~~ cells, a rotatable half wave plate (RHWP) was used to rotate the residual linear polarization to circular polarization. This also helps minimize the effect due to helicity-correlated beam parameters that arise from the residual linear polarization interacting with the photocathode. The electron beam polarization was changed in a quartet pattern of either "+ - - +" or "- + + -" with a helicity reversal rate of 960 Hz. A more detailed overview of polarized electron beam technology with references to the scientific literature on the subject is available in [13].

A double Wien filter was used to rotate the polarization of the electron beam in order to fine tune and produce fully longitudinally polarized beam during the experiment [14]. A single Wien system can flip the polarization of the beam by 90^o. In a double Wien system both Wiens can rotate polarization by 90^o which help to cancel systematic false asymmetries. This method also helped to produce ~~producing~~ fully transversely polarized beam for ancillary and background measurements. A dedicated chapter on transverse polarization measurement will be discussed later.

1.3 Accelerator

(one pass through both LINACs?)

The length of the accelerator is about 7/8 miles for one complete cycle. A thermoionic electron gun is used as the source of electron at the injector to extract electron beam of energy 67 MeV with the standard setup. The electron beam is accelerated by two linear accelerators, North and South linacs. A series of magnets bends the beam along the arcs which connects the two linacs. The beam line, transporting the beam to the three halls is shown in the Figure 1.2 (f) by the red lines. The continuous-wave (100% duty factor) electron beam from the CEBAF accelerator has a characteristic of 2 ns micro-structure that arises from the 1497 MHz Radio Frequency (RF) structure of the accelerator and the 499 MHz three-hall beam splitting scheme.

this last sentence is confusing. what structure? the bunches?

1.3.1 LINAC

(why is this not part of the above section?)

you told us this already :)

CEBAF consists of two parallel linear accelerators, each capable of approximately 600 MeV of acceleration. Electrons from the injector are sent to the north linear accelerator (linac) at an energy of 45 MeV. Superconducting niobium RF resonant cavities shown in Figure 1.2 (e) in the north linac section accelerate the electrons, in a standard tune the maximum gain in energy per linac is 600 MeV in energy. There are 20 cryomodules per linac, where each cryomodule consists of 8 cavities with an outer vacuum vessel, thermal radiation shield, magnetic shield, super insulation, and a welded helium vessel [10,15]. The beam then goes through the east arc and into the south linac to accelerate for another 600 MeV energy gain. This beam can be sent directly to the Beam Switch Yard (BSY) for distribution to the experimental halls (Figure 1.2 (a)) or the beam can be steered along the west arc for another pass through the two linacs for another 1.2 GeV of energy gain. This process can be repeated up to four times. A maximum of five passes through both linacs provide energies from 445 MeV to 5945 MeV. As the beam energies are different in each passs, a different set of magnets are used to steer the beam around the arcs after each pass. One pass beam was used for the Q-weak experiment as the required beam energy was 1.155 GeV.

Is it 67 or 45? you give us two values.

1.4 Beamline

The beamlines that transport the beam from the accelerator to the experimental halls are shown in Figure 1.2. A two meter long dipole splits the beam for three ~~diffent~~ different halls at Lambartson (Figure 1.2 (a)). Beamlines for each hall (Figure 1.2 (b)) consists of a series of quadrupole and dipole magnets to help focus/ defocus the beam along the way to the target in each hall (shown in Figure 1.2 (c) for Hall-C). The beam position, profile and current were measured at various points along the Hall-C beamline using BPMs (Figure 1.2 (c)) and BCMs respectively. A part of Hall-C beamline also forms an arc, the bending magnets of the Hall-C arc were used to measure the relative beam energy with a precision of $\Delta E/E \approx 10^{-4}$ (details in Section 1.5.4). A details sketch of Hall-C beamline elements provided by this author can be found in [16].

I've never seen anyone use this term before. Perhaps just leave it out? Or re-print as an appendix, perhaps?

1.5 Beam Monitoring

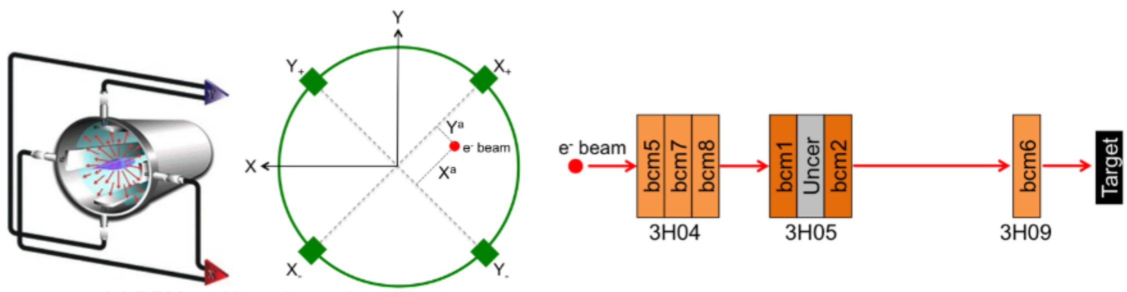

(a) BPM and its schematic

(b) BCMs in Hall-C beamline

Figure 1.4 Beam position and current monitors. (a) Beam Position Monitors with four antennae rotated by 45^o in the plane. Z axis is perpendicular to the plane. (b) Beam Current Monitors and its their location schematics at Hall-C.

1.5.1 Beam Position Monitor

Seems repetitive

The beam position was continuously monitored at many places along the Hall-C beamline and throughout the accelerator by beam position monitors (BPM) during data collection to ensure that the beam was centered on the target. Each beam position monitor consists of a resonant cavity of a fundamental frequency equal to that of the accelerator and the Hall C beam. The position of the beam is measured using four antennae rotated by 45^o in the plane (y axis is in direction opposite to gravity, x is horizontal) perpendicular to beam direction (z-axis) shown in Figure 1.4 (a). Four antennae inductively pick up the fundamental frequency of the beam as it passes through [the] BPM. Then radio frequency (RF) signal from each antena (wire) is processed electronically which yields a DC signal proportional to the beam current times the distance between the wire and the beam. DC signals were sent through voltage-to-frequency converters and recorded with scalers that are read out by Experimental Physics Industrial Control System (EPICS), the system used by the accelerator and end stations for slow control and monitoring of accelerator and experiment parameters with the rest of the data from the experiment. The beam position X^a and Y^a along the axis of the wires are calculated by a difference over sum of each opposite wire as:

Are you sure about this? EPICS is slow and not used for detailed analysis. I believe we had scalers in the Qweak Racks as well as VQweaks read out the beamline elements.

$$X^a = k\frac{(X_+ - X_{offset+}) - \alpha_X\,(X_- - X_{offset-})}{(X_+ - X_{offset+}) + \alpha_X\,(X_- - X_{offset-})} \tag{1.5.1}$$

Where $X_{offset+(-)}$ is the offset for the $X_{+(-)}$ wire, k is the sensitivity of the BPM at 1497 MHz and α_X is a measure of the possibly different gain between the X_+ and X_- antennae [17, 18]. The gain difference α_X is defined as

$$\alpha_X = \frac{X_+ - X_{offset+}}{X_- - X_{offset-}} \tag{1.5.2}$$

The center of gravity of the four antenna signals measures relative changes in the offset of the beam from its ideal trajectory. Same approach is used to compute relative beam position Y^a. Then the position of the beam in hall co-ordinate system can be written as:

$$\begin{pmatrix} X \\ Y \end{pmatrix} = \frac{1}{\sqrt{2}}\begin{pmatrix} 1 & -1 \\ 1 & 1 \end{pmatrix}\left[\begin{pmatrix} X^a \\ Y^a \end{pmatrix} - \begin{pmatrix} X^a_{offset} \\ Y^a_{offset} \end{pmatrix}\right] \tag{1.5.3}$$

The information from BPM for a event can not be understood as the exact beam position on target for that event, as the signals are not synchronized with the event data itself and also the actual position on target is constantly changing due to the fast raster system. Practically, an average beam position is calculated using a rolling average of BPM data information a specified number of previous events, the appropriate choice of which depends on the experiment data rate, and this average beam position is then corrected for each event using the fast raster signals [19]. Normally average beam position on target is very stable over the period of a single CODA run, it is more practical to simply ignore the event-by-event BPM information and fix the average beam position as a parameter of the analysis, and to use the raster signals to measure the change in beam position relative to the fixed average position. BPMs were calibrated using the super harps in Hall-C beamline [20]. Typically calibrated BPMs has a resolution of 1 μm. More details about BPM resolution will be discussed in analysis chapter. Basic details about BPMs can be found in [21].

more basic than this? If so, why mention it. If more, then not basic :)

Six BPMs in the Hall-C beamline over a span of 10 m upstream of the target were used to project the beam path at the Q-weak target continuously during the experiment. Error averaged postion changes over six BPMs were used to measure the position and angle changes at the target, where BPMs in front of the target were used for the same to verify the result. Detail description about the target BPM can be found in a technical document by this author [22] and Buddhini's thesis [23].

??. use last names

Use only one term for the target. Either "Qweak target" always or just target

1.5.2 Superharp

A more precise and accurate determination of the beam position and profile is obtained using the superharp system. Each superharp consists of a set of two vertical wires and one horizontal wire strung on a moveable frame. These wires can be scanned across a low current beam to measure its profile and absolute position. The signals induced on the wires as they are scanned across the beam are digitized by an analog to digital converter (ADC) and correlated with the wire positions as recorded by an encoder equipped with absolute position readout electronics. Since a harp scan interferes destructively with the electron beam, data taking must be interrupted to perform the measurement. In addition to measuring the beam profile, the superharp system provided a reference coordinate against which the BPMs were calibrated.

1.5.3 Beam Current Monitor

Čerenkov detector yields were normalized with beam current monitors to remove charge fluctuation . A series of six beam current monitors (BCMs) were used continuously for relative measurement of the beam current in the Hall-C beamline (as shown in Figure 1.4 (b)). The BCMs were coupled cylindrical stainless steel resonant cavities [24, 25] whcih were used to measure the beam current by measuring resonance of the TM_{010} mode at 1497 MHz. This signal then converted to a voltage in a RMS-DC voltage converter and read by TRIUMF made ADCs. This voltage signal also sent to a 1 MHz voltage to frequency (V-F) converter and scalers for event-mode normalization. At the beginning of the experiment only BCM1 and 2 were available. BCM 5-8 were built with low noise digital receiver then implemented during latter half of the experiment. BCM1 and 2 were absolutely calibrated using the Unser monitor ~~between them~~. The detector yields were normalized with BCM1 and 2 during Run-I and BCM8 during Run-II. Nominal current measured by these BCMs during experiment was 180 μA. More details about BCMs used during the Q-weak experiment is discussed in a technical report by Ramesh Subedi [26].

Did you ever give us reason to suspect what BCM1 and 2 mean? why no 3-4? Just say: In the beginning we had two BCM's (1,2) and later (5,6,7,8) added...

1.5.4 Beam Energy

Absolute beam energy was measured to know the initial beam energy before scattering and ??? energy asymmetry was measured to remove false asymmetry.

why would't we want to always know absolute beam energy? Why justify having to know it?

1.5.4.1 Absolute Beam Energy

The Hall-C beamline arc was used as a spectrometer to measure the absolute beam energy [28]. An electron passes through an arc changes its momentum and can be expressed as

$$p = \frac{e}{\Delta\theta} \int Bdl \tag{1.5.4}$$

where $\Delta\theta$ is the change in bending angle through the arc and $\int Bdl$ is the magnetic field integral over the electron path. Three set of superharp scanners [29] were used to determine the position and the angle by scanning the beam at the beginning, end, and middle of the arc. All the active (what active elements?) elements of the beamline were turned off to avoid any distortion. This procedure is an invasive process and needed dedicated measurements. A typical energy measurement using this method yield energy as 1160.39 ± 1.74 MeV [15]. [So is this a calibration? or are you saying we only measure absolute beam energy and then never know it again?]

1.5.4.2 Energy Asymmetry

One of the helicity correlated beam parameter is beam energy asymmetry. Small changes in the energy asymmetry could result into false asymmetry, hence precise measurement of the energy asymmetry was important for ~~the~~ Q-weak. ~~Inside the Hall-C beamline,~~ In the middle of the arc near the region of 3C12 has the highest dispersion. Any change in beam energy could result a big
did you ever tell us what this was?
horizontal position change in the 3C12. Then relative energy change at the target can be expressed as

$$\left(\frac{\Delta E}{E}\right)_{target} = \frac{1}{M_{15}}\Delta X_{3C12} - \frac{M_{11}}{M15}\Delta X_{target} - \frac{M_{12}}{M_{15}}\Delta X'_{target} \tag{1.5.5}$$

where ΔX_{3C12}, ΔX_{target}, $\Delta X'_{target}$ are position change at 3C12, position change at target, and angle change at the target respectively. First order beam transport matrix between 3C12 and target M_{11}, M_{12}, and M_{15} were determined using OPTIM [30]. This calculation works for linear models and any residual dispersion at the target or X-Y coupling are not considered in this first order calculation. More details about this model will be discussed in the following chapter. Typical energy asymmetry at the target during the experiment was $\mathcal{O}(1)$ ppb. A technical note with more details from this author on how beam energy changes was identified in Q-weak can be found [27].

???

It just seems to me like you break things down into too many sub-sections without needing them. Also, you keep refering to you as "this author" as if we forgot whose thesis we were reading :)

1.5.5 Beam Modulation

The e-p scattering rate in first order depends on five beam parameters: horizontal position (X), angle (X'), vertical position (Y), angle (Y'), and beam energy (E). Changes in these beam parameters when the beam polarization is reversed will create false asymmetries. Although different technique were used to keep helicity-correlated parameter changes as small as possible, ~~most~~ we still need to correct for ~~such~~ any false asymmetries. To do this, X, X', Y, Y' were modulated using four air-core dipoles in the Hall C beamline and beam energy was modulated using a superconducting RF cavity. The goal of the beam modulation system was to occasionally induce controlled beam parameter changes ΔX_i, measure the resulting detector false asymmetry A_{false}, and determine the detector sensitivities $\partial A/\partial X_i$. This will allow later correction of beam false asymmetries via

$$A_{false} = \sum_{i=1}^{5} \frac{\partial A}{\partial X_i} \Delta X_i \tag{1.5.6}$$

Even if these corrections prove to be small under ideal running conditions, the modulation system will allow to determine any undesirable changes [31]. A dedicated chapter on beam modulation system and contribution from this author will be discussed in following chapter.

1.5.6 Halo Monitors

Another important property of the beam is ~~halo~~ the beam halo, which refers to stray electrons that move along with the primary beam but are sufficiently far from the beam center and can contribute in the background. why are they background? Beam halo can be generated via space-charge effects from of electrons during bunching, scraping in the beam pipe, or poor vacuum and can be measured using plastic Lucite detector and scintillation counters. Apertures on the halo target were 8 mm square openings and 13 mm diameter hole. An 8 mm square opening and 13 mm diameter hole were used as halo targets. The halo monitors were located immediately downstream of the halo targets and upstream of the Q-weak LH_2 target. The beam halo can also be estimated using the main detectors and luminosity monitors which can be normalized using the hole targets.

This is almost the exact same sentence as before.

1.6 Polarimetry

experimental [remember, hadronic structure is the largest, by far]

The most dominant systematic experimental uncertainty for the Q-weak experiment is expected to come from a 1% absolute uncertainty on beam polarization as shown in Table 1.1. In order to achieve this goal

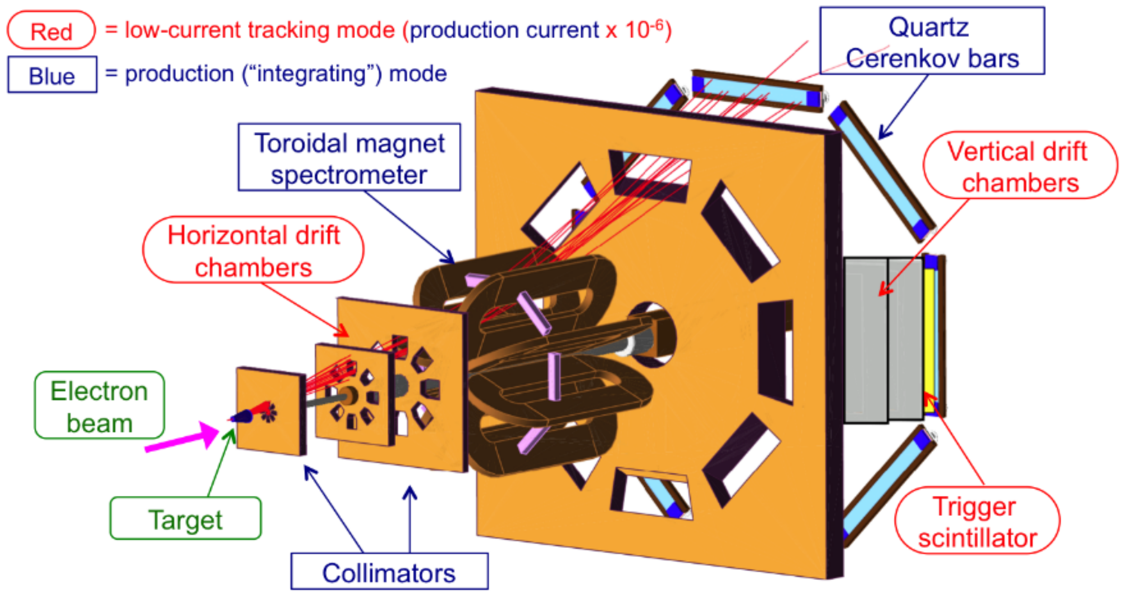

Figure 1.5 Schematic diagram of the Q-weak apparatus. The basic experimental design showing the target, collimators, toroidal magnet coils, electron trajectories, and detectors. Elastically scattered electrons focus at the Čerenkov detectors. High current production mode apparatus components are shown in blue rectangular boxes and low current tracking mode components are shown in red elliptical boxes. Beam direction is from left to right.

two polarimeters, well tested invasive low current Møller polarimeter and noninvasive relatively new Compton polarimeter were used to measure the beam polarization.

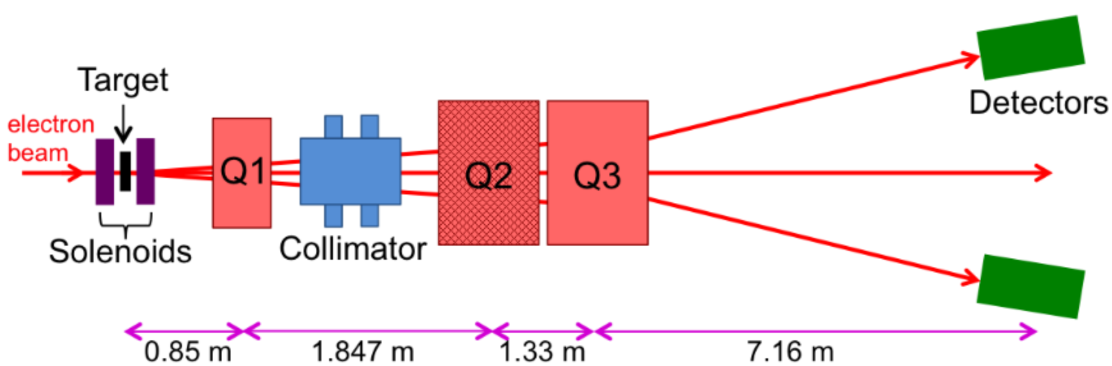

Figure 1.6 Layout of the Hall C Moller polarimeter showing tin foil target, set of superconducting solenoids, quadrupoles (Q2 was off during Q-weak), collimator box, and symmetric detectors.

1.6.1 Moller Polarimetry

The Møller polarimeter is used to measure the polarization of the longitudinally polarized electron beam entering Hall-C [33]. To accomplish this goal, the polarimeter measures the spin-dependent asymmetry in the cross section for the elastic scattering of polarized electrons from polarized electrons i.e. $e^- + e^- \rightarrow e^- + e^-$(Møller scattering). This is a pure Quantum Electrodynamics (QED) process and its cross section can be calculated accurately. The target used for the scattering is a thin foil of iron magnetized by superconducting solenoids with field of ~4 T. A set of quadrupole magnets Q1 and Q3 were used (Q2 was off during the experiment[1]) to focus the scattered and recoiled electrons in to the symmetric detectors in coincidence. Then detectors measure the asymmetry and then compute the polarization after correcting for the backgrounds. Figure 1.6 shows the layout of the Hall-C Basel Møller polarimeter. It was designed to operate with currents lower than 8μA whereas Q-weak production current was 180μA. During the experiment, Møller measurements were performed invasively at low currents (1μA) three times a week. The typical ~~Typical~~ measured longitudinal polarization using the Møller polarimeter was about 88%. A sample of the Møller result will be shown in later chapters. More elaborated description of the Møller polarimeter can be found in Matthias Loppacher's thesis [34] and polarization technique used during Q-weak can be found in Rakitha's [35] thesis.

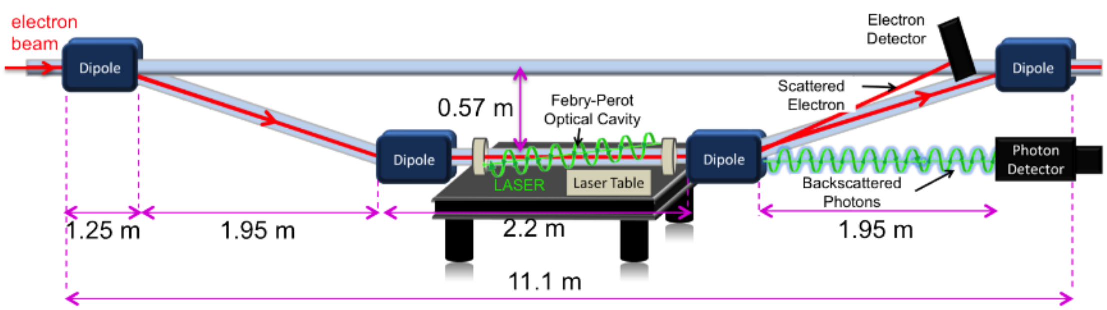

Figure 1.7 Schematic of the Hall-C Compton polarimeter. The incoming electron beam interacts with the green LASER at the straight section of the chicane. The scattered electrons and back-scattered photons are detected by electron detector and photon detector respectively for each helicity (MPS) state.

[1]some beamline optics survey suggested leakage current in Q2 and will be discussed in details in latter chapter

1.6.2 Compton Polarimetry

A new Hall-C Compton polarimeter was installed and used for the Q-weak experiment [36]. This was a noninvasive high current (180 μA) polarimeter and continuously took data during production data taking. The apparatus for the Compton polarimeter includes four dipoles in a chicane, a green LASER, an electron detector, and a photon detector as shown in Figure 1.7. Compton polarimeter use the Compton scattering of the incident electron beam with photons from a green LASER. The scattered electrons and back-scattered photons provides two independent measurement of the polarization using electron and photon detector respectively. The dipole chicane were used to move the interaction point away from primary beam in order to detect back-scattered photons in the photon detector. A CsI crystal with photo multiplier tube was used as photon detector. Latter in the experiment germanium silicon oxide (GSO), and led-tungstate ($PbWO_4$) were used instead of CsI in the photon detector. The electron detector consist radiation hard diamond micro-strips and for the first time used as a tracking device in an experiment. The scattered electrons were detected in a array of 96 diamond strips after third dipole. There were four detector planes, each with 200 μm thick 96 strips, and were controlled by four VME 1495 board. The measured beam polarization using Compton polarimeter was about 87-89%. A sample of Compton result will be shown in later chapters. More detailed description of Compton polarimeter and its electron and photon detector measurements will be discussed by Amrendra Narayan [37] and Juan Carlos Cornejo [38] respectively in their future theses.

1.7 Targets

The Q-weak target system has two main components: a main liquid hydrogen (LH_2) cell for production data taking and a matrix of solid targets used for background measurements and ancillary tests. Solid target ladder was thermally coupled to the bottom of the LH_2 cell. A schematic of the Q-weak target system is shown in Figure 1.8.

1.7.1 Liquid Hydrogen Target

A 34.4 cm long liquid hydrogen (LH_2) cell was used as primary target for the Q-weak experiment [39]. This target can dissipate 2.5 kW of power deposited by the 1.155 GeV, 180 μA, 4 mm $\times$ 4 mm rastered electron beam and is highest power cryogenic target in the world to date. A unique hybrid cooling system at JLab namely End Station Refrigerator (ESR) for 15 K coolant and Central Helium

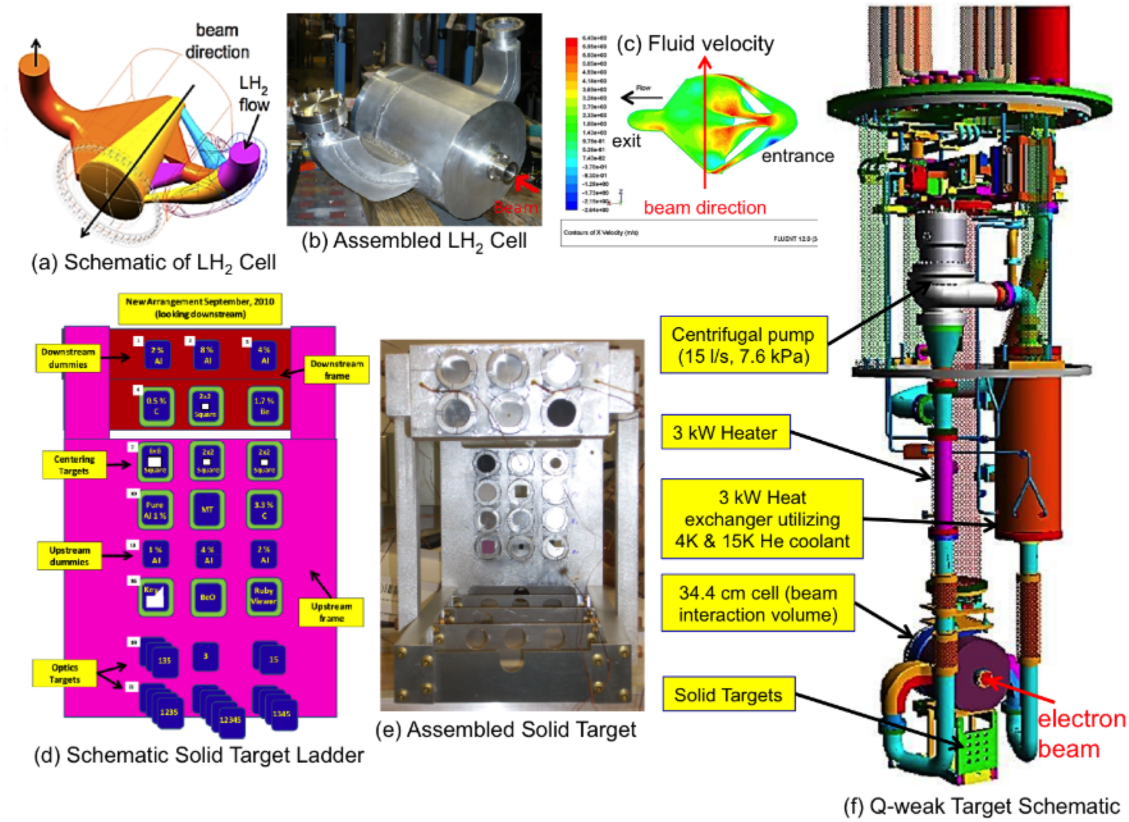

Figure 1.8 Q-weak target system. (a) Canonical shaped (Computer Aided Drawing) (CAD model of target cell design. (b) Assembled LH_2 target cell. (c) Simulation of LH_2 velocity contours inside target cell using CFD. (d) Schematic of solid target ladder. (e) Assembled solid target. (f) Full schematic of Q-weak target. Along with main LH_2 target cell, pump, heater, heat exchanger, solid targets are shown.

Liquefier (CHL) for 4 K coolant were ~~used as~~ mixed at the heat exchanger (Figure 1.8 (f)). A high power heater was used to replace the heat deposited by the electron beam in case of beam trips. It also helped to stabilize the LH_2 target temperature in conjunction with 15 K and 4 K coolant in a proportional integral derivative (PID) feedback system. The ~~LH_2~~ (55 liters) of LH_2 was ~~was~~ contained within a target cell of thin aluminum (Al) alloy window and was operated under 35 psi pressure at 20 K temperature and with a transverse flow of 1.2 kg/s maintained by modified automobile centrifugal turbo pump at frequency of 30 Hz.

This long ~~target~~ cell with canonical shaped (Figure 1.8 (a,b)), accommodated our required 7.9^o scattering angle, helped to achieve the high luminosities and hence the statistical goal. The current mode production data taking ~~with Čerenkov detectors made experiment~~ was very sensitive to target density fluctuation, ~~The~~ as such, the target was designed using Computational Fluid Dynamics (CFD) and simulated using ANSYS [40] (a fluid dynamics simulation code) to minimize noise from density fluctuations and maintain nominal fluid density. The simulation shows the main hot spots were entrance and exit windows of the cell as shown in Figure 1.8 (c). The exit window was 0.02 inch thick aluminum alloy with a 10 inch radius of curvature and a 0.005 inch nipple to minimize backgrounds.

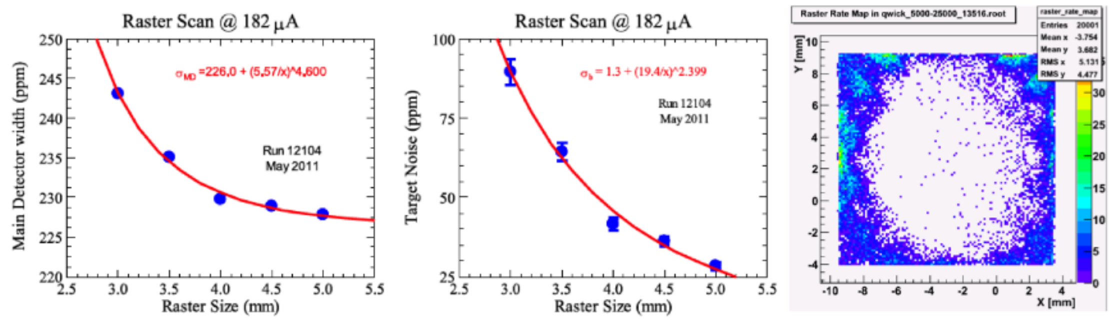

(a) Main detector vs raster size (b) Target boiling noise vs raster size (c) Raster rate with hole target

Figure 1.9 Raster scan. [15]

1.7.1.1 Raster

The intrinsic size of the electron beam (perpendicular to beam direction) at JLab is ~2 μm and creates localized high power density on the LH_2 target. This could result in boiling the target. ~~The~~ Hence, the beam was rastered ~~over~~ on ~~an area of~~ the target ~~of~~ over an area of up to 4 mm $\times$ 4 mm by the fast raster ~~to reach~~ system. acceptable beam currents without damaging the target and to reduce the effect of localized boiling ~~in LH_2 target~~. The raster was designed to have a matching beat frequency with fast helicity flip of 960 Hz. This method assures each integration period has the same complete raster pattern on the target and prevents systematic differences in the beam position between Macro Pulse Signal (MPS). what is MPS??? The contribution of target density fluctuation and raster size dependence to the statistical width was measured by using known detector asymmetry widths from statistics and other sources (shown in Figure 1.9 (a)). In typical production running with 180 μA, 4 mm $\times$ 4 mm rastered beam the contribution from target boiling noise was 46 ppm (shown in Figure 1.9 (b)), which is relatively small contribution to the statistical width of ~200 ppm.

1.7.2 Solid Target

Along with LH_2 target an array of solid targets [41] consist of aluminum (Al) dummy targets, optics targets, and centering targets were used for background and ancillary measurements. The solid target ladder was thermally coupled to the bottom of the LH_2 cell as shown in Figure 1.8 (f). A detailed schematic of solid target matrix looking upstream is shown in Figure 1.8 (d,e). Horizontal and vertical motion controller were used to insert different targets into the beam. Three different Al dummy target thicknesses for both upstream and downstream locations were used to measure the effect of radiative corrections in the measured asymmetry. The optics targets were primarily used for particle origin reconstruction in the tracking measurements. Optics target helped to locate the position of the target ladder in raster rate scan as shown in Figure 1.9 (c).

1.8 Collimators and Shielding

A set of three lead collimators were used to define the experiment's angular acceptance and minimize the inelastic and neutral background contribution to the detector ~~rate~~. ~~The first collimator was placed just downstream of the target.~~ The collimator system is shown in Figures 1.5 and 1.10 (c). The first collimator, a water cooled tungsten plug of inner radius ∼7 mm, was placed just downst.... and was used to reduce the electron scattering from the beamline ~~Al~~. The second (or primary) collimator defined the acceptance as 4% of π in θ and 49% of 2π in ϕ. The angular acceptance of the primary collimator from the upstream end of the target window is θ = 5.8^o - 10.2^o and θ = 6.6^o - 11.5^o from the downstream end. The third collimator was before QTor and further cleaned the electron flux before it reached what's QTor? to QTor magnetic field. Besides these three collimators a 80 cm thick shielding wall of barite-loaded (Ba_2SO_4) high-density (2.7 g/cm^3) concrete was used after QTor for addition shielding. A details description of shield wall and collimator system can be found in Juliette [42], and Katherine's [15] theses.

1.9 Q-weak Toroidal Magnetic Spectrometer: QTor

The eight fold symmetric torodial magnetic spectrometer used for the Q-weak experiment is known as QTor (shown in Figure 1.10 (a,d)). It has race track shaped what's that?? water cooled copper (iron free) magnetic coils (shown in Figure 1.10 (e)). The dimensions of the each magnet coil are 2.2 m long along the straight section, 0.235 m of inner radius, and 0.75 m of outer radius. Eight such identical coil packages with $\Delta\phi \sim 45^o$ gaps between them made the QTor structure (relevant coordinate system is shown in Figure 1.10 (b)). The primary objective of QTor magnet was to to focus the elastically scattered electrons to the main Čerenkov detector in the focal plane of the asymmetry measurement (shown in Figure 1.10 (c)). During nominal elastic asymmetry measurement QTor was operated at 8921 A whereas during inelastic ($N \rightarrow \Delta$) asymmetry measurement the operational

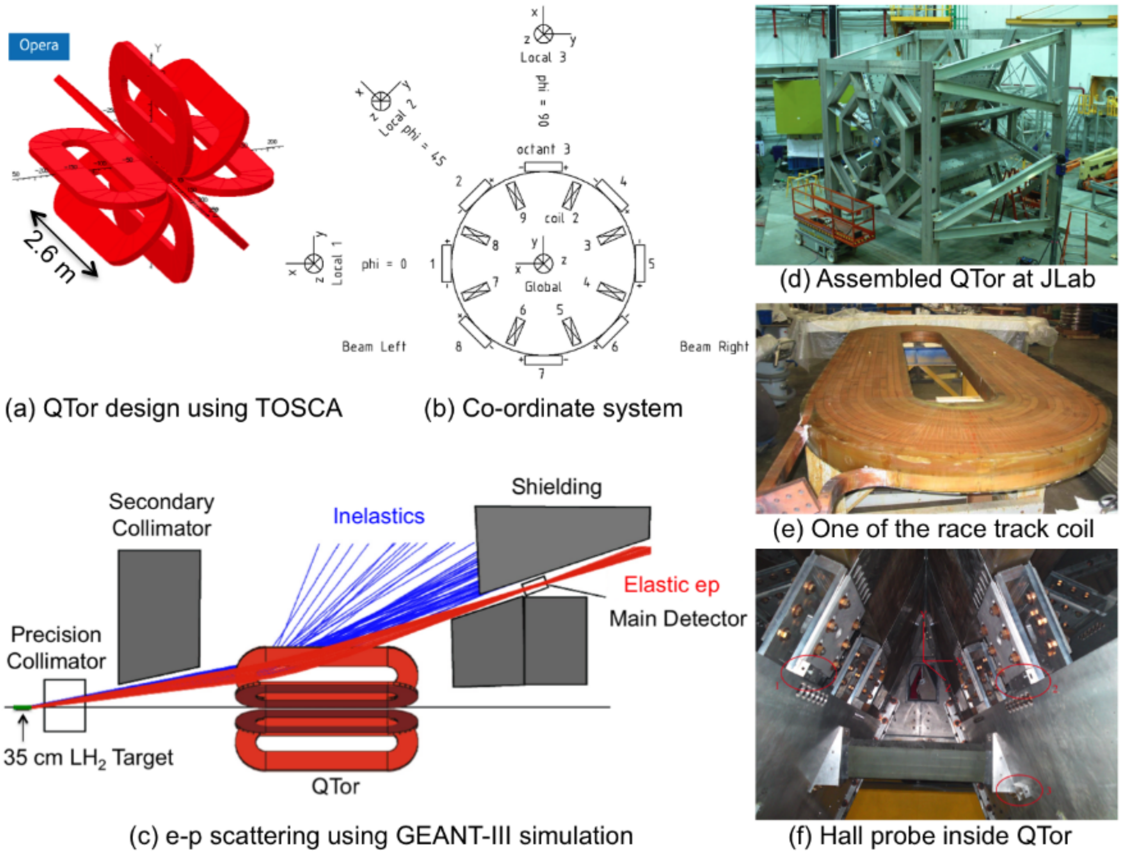

Figure 1.10 Q-weak torodial magnetic spectrometer (QTor). (a) QTor design using TOSCA. (b) Co-ordinate system. (c) e-p scattering using GEANT-III simulation. (d) Assembled QTor at JLab. (e) One of the race track coil. (f) Hall probe inside QTor.

current was 6700 A. The magnet required a 10 kA power supply at 130 V and produced a field integral $\int \vec{B} \cdot d\vec{l} = 0.67$ T.m ~??? along the central trajectory. Peiqing Wang has ~~described~~ more details about the QTor design structure and field map in his master's thesis [43].

1.9.1 Hall Probe

A transverse (LakShore MNT-4E02-VH) hall probe was used to measure the online QTor magnetic field. Three hall probe mount panels were designed and attached to the inside wall of QTor as shown in Figure 1.10(f). The ~~Hall~~ probe was inserted ~~slide~~ inside the mount and attached with a LakeShore 460 3-channel Gaussmeter controller via a 30 m long special magnetically shielded cable (MPEC-100). A VME IOC was then connected with the controller in order to control the system remotely via a CPU (vmec18). EPICS controls were used as a ~~for this~~ live control and read ~~read~~ back system via the active

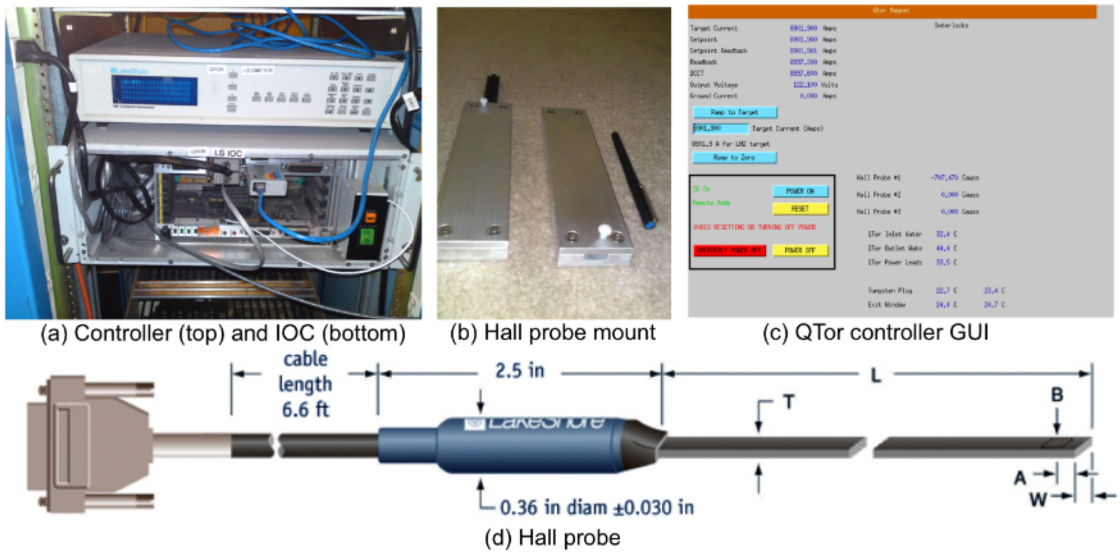

Figure 1.11 QTor controls and hall probe. (a) Lakeshore controller and IOC. (b) Hall probe mount. (c) QTor controller GUI. (d) Hall probe.

EPICS channel Q1HallP. More details about design and functionality of QTor hall probe can be found in [44]

would anyone outside Qweak know what this means?

1.10 Detector System

The Q-weak detector system consists of main Čerenkov detectors and two set of luminosity monitors.

1.10.1 Main Čerenkov Detectors

The Q-weak main detectors are 200 cm × 18 cm × 1.25 cm fused silica Čerenkov quartz bars. The QTor magnetic spectrometer focuses elastically scattered electrons into the eight main detector bars azimuthally oriented around the beamline (Figure 1.12 (b,c)). Didn't you say this in the QTor section? Each detector consists of 100 cm long quartz bar optically coupled together and at each end of the bar, a 5 cm diameter photo-multiplier tube (PMT) also optically glued outside of electron flux (shown in Figure 1.12 (a)). ??? Electrons entering the quartz produce a cone of Čerenkov light that undergoes through total internal reflection and then gathered at each end of the bar with PMTs. The silica was chosen for its radiation hardness and low scintillation. why low? A lead (Pb) pre-radiator was installed in front of the main detectors to improve elastic electron light yield and reduce neutral background. More details description of

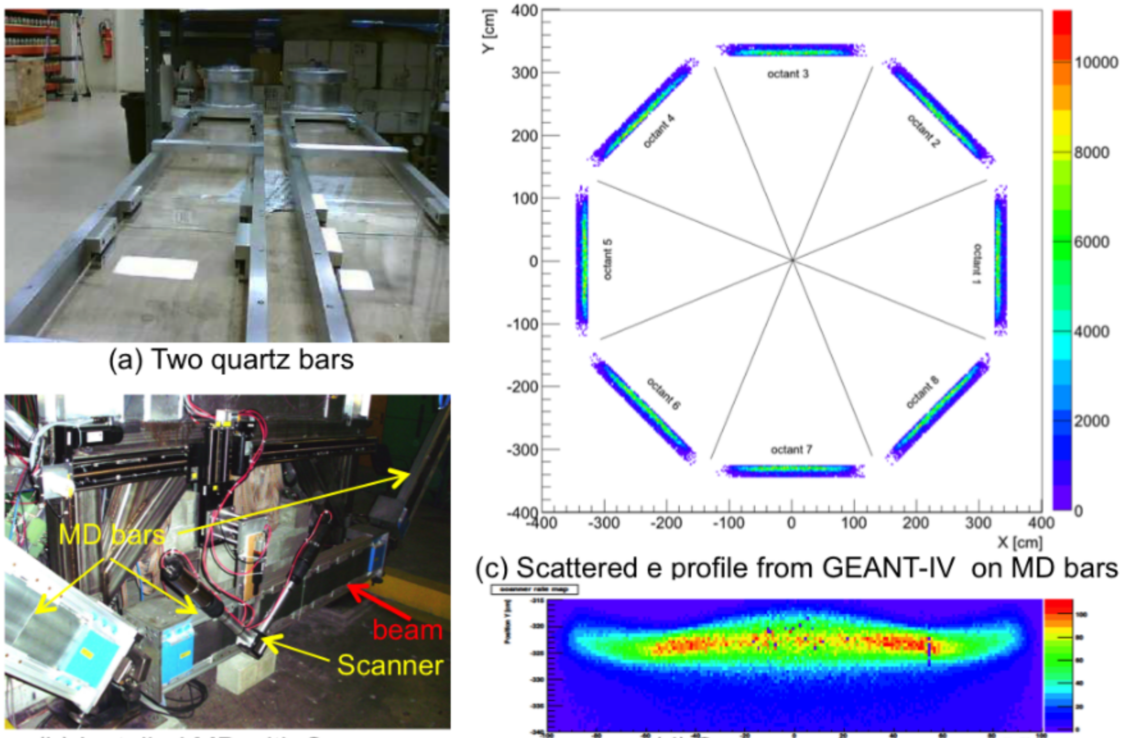

(a) Two quartz bars
(b) Installed MD with Scanner
(c) Scattered e profile from GEANT-IV on MD bars
(d) Scanner rate map

Figure 1.12 Q-weak main Čerenkov detector system. (a) Two quartz bars. (b) Installed main detectors at Hall-C. (c) A GEANT-IV simulation showing elastic scattered electron profile on the quartz bars [45].

~~main~~ the Čerenkov detector development, construction, and installation can be found in Peiqing Wang's thesis [46].

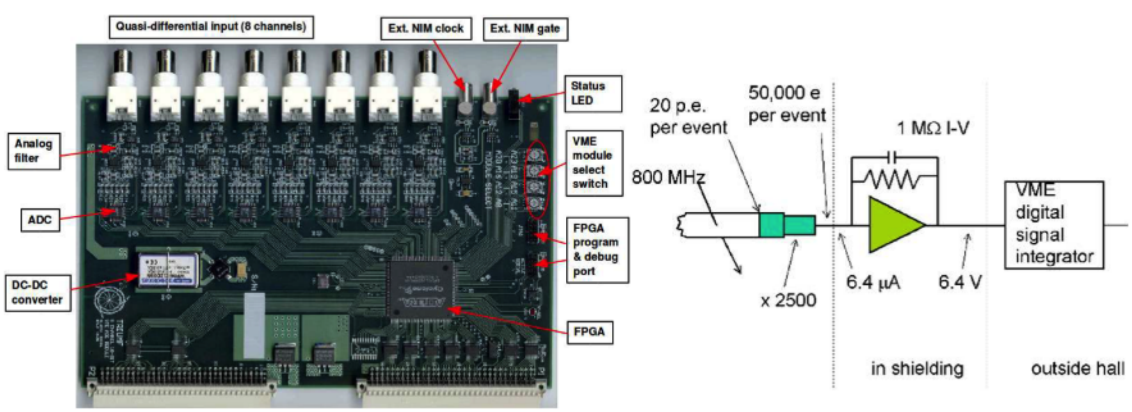

(a) 18 bit TRIUMF ADC
(b) Schematic of the current mode signal chain

Figure 1.13 ADC

1.10.1.1 Low Noise Electronics

In order to achieve the desired statistical uncertainty low noise electronics were designed and built by TRIUMF and consist of low noise current-voltage preamplifiers and digitizing integrators. The preamplifiers convert the DC anode current coming from the PMTs to a voltage ~6 V signal for nominal production running. This signal is then digitized by 18-bit analog to digital converters (ADCs) to integrate at a sampling rate 500 kHz.

This is confusing sounds like we integrate at 500kHz. Rather, we sample at 500 kHz and integrate at ~1kHz. maybe rewrite it.

1.10.1.2 Focal Plane Scanner

A focal plane scanner was used to measure the beam profile in both high current production running and low current tracking mode in order to test systematic effects like target density change. Two 1 cm×1 cm×1 cm fused silica quartz radiator overlapped in a "V" shaped and signals were read by individual PMTs in the scanner. This scanner system is then mounted on MD octant 7 (as shown in Figure 1.12 (b)) for beam profile scan. One example of such scan at 50 μA beam current with LH2 target is shown in Figure 1.12 (d). Jie Pan has described in details about the construction, schematic and analysis of focal plane scanner in her thesis [47] ← Funny story. It didn't work. Do you really want it in your thesis?

1.10.2 Luminosity Monitors

The luminosity monitors, like the main detectors, were based on fused silica Čerenkov radiators and with a light guide flushed with nitrogen gas to minimize corrosion. Two types of azimuthally symmetric luminosity monitors were used as beam diagnostic tools for the Q-weak experiment. The upstream luminosity monitors were located on the front face of the primary collimator 5 m from the target (shown in Figure 1.14 (a)) and the downstream luminosity monitors are located 17 m downstream of the target and very close to the beam dump area (shown in Figure 1.14 (b)). Both lumis were expected to detect electrons from small angle electron-proton and electron-electron scattering with an anticipated null asymmetry (ppb-level asymmetry). Upstream lumis were extremely useful for estimating beamline backgrounds. In some cases the measured asymmetry by the lumis were not as small as expected and and were also time dependent. Examples will be discussed in a later ~~analysis~~ chapter. More detailed description of luminosity monitors and analysis can be found in John Leacock's thesis [48].

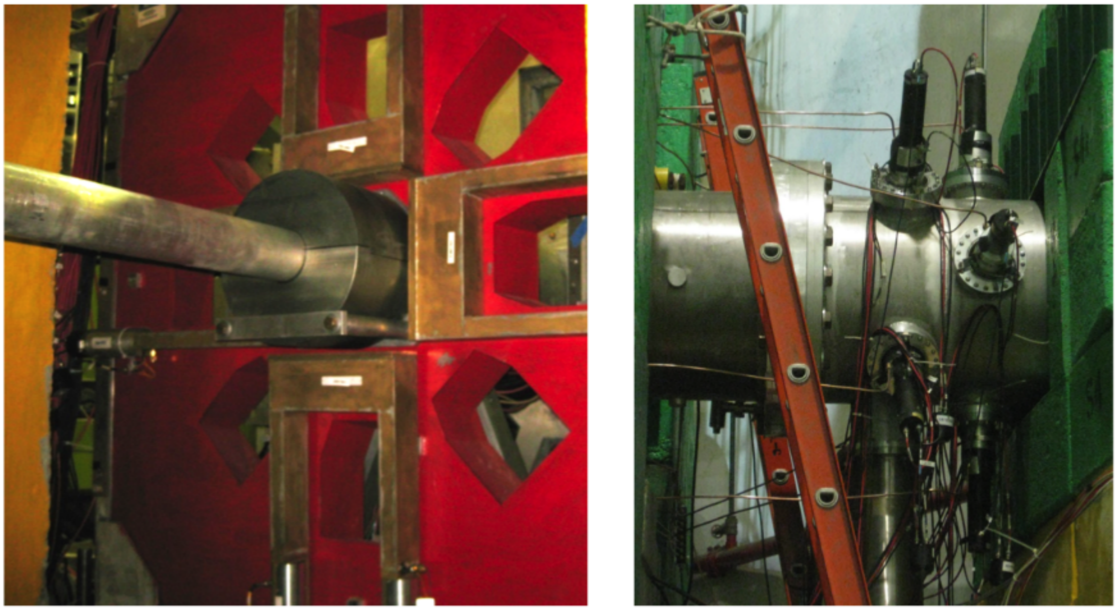

(a) Upstream luminosity monitors (b) Downstream luminosity monitors

Figure 1.14 Luminosity monitors.

1.11 Tracking Detector System

The asymmetry of the elastically scattered electron is approximately proportional to the four momentum transfer squared, Q^2 (details in Equation ??). A tracking system was necessary to measure Q^2 with 0.5% relative uncertainty as proposed by the experiment 1.1. A pair of horizontal drift chambers (HDCs) in region 2 (R2) were used to determine the scattering angle θ with an angle resolution of ∼0.6 μrad and particle trajectory with a position resolution ∼200 μm (as shown in Figure 1.5). Four set of vertical drift chambers (VDCs) and two trigger scintillators were used upstream of the target (shown in Figure 1.5) in region 3 (R3) to measure Q^2. Detector packages in R2 and R3 can be rotated into each MD octant pair using a mechanical rotor to measure ~~the~~ any octant dependence. Relation of Q^2 with θ is shown in Equation 1.1.3. The tracking system operated at ∼6 order of magnitude smaller beam current than parity production current. A details description of tracking system can be found in Jie Pan's thesis [47].

Not quite. R2 measures Q² with the angle already. R3 tracks to MDs to define Q² as seen by the MD's.

1.12 Data Acquisition

?? analog??

The CEBAF Online Data Acquisition (DAQ) or CODA software system convert physical signals into digitized signals in order to handle and store for future analysis. Two ~~set of~~ independent DAQ low current was also used for related non-tracking tasks (i.e. Al studies).

~~systems~~ configurations were used for the experiment: integration mode for high current production data taking and counting mode more low current ~~tracking~~ measurements. The data taking during integration mode was triggered by the MPS signal from the accelerator with frequency of 960 Hz and trigger scintillators were used ~~to~~ as the trigger for the event mode running. A software prescale factor was used to control how often the DAQ was triggered by the specific trigger for each hardware trigger. Several read out controllers (ROCs) were used to install different subsystem electronics?? The CODA system used ethernet to communicate with all the ROCs. The Event Builder (EB) system was used to generate complete event from data fragments read from ROCs and the Event Transfer (ET) system provided central access to data events for multiple clients at real-time. During Q-weak experiment ~40 TB of raw data were collected. The averaged data, such as yields, asymmetries, differences, HWP state, target, regression slopes, flags for data quality, ~~are~~ were saved ~~using~~ to a MySQL database. Buddhini [23] and Rakitha [35] provided more technical details on data acquisition ~~on~~ in their theses.

Seems good. Though, I find it odd that each chapter is a subsection. I would cut down the number of subsections and just use more chapters. This will help cut down the repetativeness of having to always introduce your section.

Also, be careful with jargon. What is a lumi? Why do you repeat Qweak target? Aren't they all Qweak targets? Why is Region 2, 3 important? Where is Region 1? What in the world is 3C12? Who is "this author" that you speak of? :)

REFERENCES

[1] Thomas Jefferson National Accelerator Facility. http://www.jlab.org/.

[2] Q weak Collaboration. The Q-Weak Experiment: A search for New Physics at the TeV Scale via a Measurement of the Proton's Weak Charge. E02-020 proposal, December 2001.

[3] Q weak Collaboration. The Q-weak Experiment: "A Search for New Physics at the TeV Scale via a Measurement of the Proton's Weak Charge". E05-008 jeopardy proposal, December 2004.

[4] Q weak Collaboration. The Q-weak Experiment: "A Search for New Physics at the TeV Scale via a Measurement of the Proton's Weak Charge". E05-008 jeopardy proposal, December 2007.

[5] E.J. Beise, M.L. Pitt, and D.T. Spayde. The sample experiment and weak nucleon structure. *Progress in Particle and Nuclear Physics*, 54(1):289 – 350, 2005.

[6] D. S. Armstrong, J. Arvieux, R. Asaturyan, T. Averett, S. L. Bailey, G. Batigne, D. H. Beck, E. J. Beise, J. Benesch, L. Bimbot, J. Birchall, A. Biselli, P. Bosted, E. Boukobza, H. Breuer, R. Carlini, R. Carr, N. Chant, Y.-C. Chao, S. Chattopadhyay, R. Clark, S. Covrig, A. Cowley, D. Dale, C. Davis, W. Falk, and J. M. Finn. Strange-quark contributions to parity-violating asymmetries in the forward g0 electron-proton scattering experiment. *Phys. Rev. Lett.*, 95(9):092001, Aug 2005.

[7] K. A. Aniol, D. S. Armstrong, T. Averett, H. Benaoum, P. Y. Bertin, E. Burtin, J. Cahoon, G. D. Cates, C. C. Chang, Y.-C. Chao, J.-P. Chen, Seonho Choi, E. Chudakov, B. Craver, F. Cusanno, P. Decowski, D. Deepa, C. Ferdi, R. J. Feuerbach, J. M. Finn, S. Frullani, K. Fuoti, F. Garibaldi, R. Gilman, A. Glamazdin, V. Gorbenko, J. M. Grames, J. Hansknecht, D. W. Higinbotham, R. Holmes, T. Holmstrom, T. B. Humensky, H. Ibrahim, C. W. de Jager, X. Jiang, L. J. Kaufman, A. Kelleher, A. Kolarkar, S. Kowalski, K. S. Kumar, D. Lambert, P. LaViolette, J. LeRose, D. Lhuillier, N. Liyanage, D. J. Margaziotis, M. Mazouz, K. McCormick, D. G. Meekins, Z.-E. Meziani, R. Michaels, B. Moffit, P. Monaghan, C. Munoz-Camacho, S. Nanda, V. Nelyubin, D. Neyret, K. D. Paschke, M. Poelker, R. Pomatsalyuk, Y. Qiang, B. Reitz, J. Roche, A. Saha, J. Singh, R. Snyder, P. A. Souder, R. Subedi, R. Suleiman, V. Sulkosky, W. A. Tobias, G. M. Urciuoli, A. Vacheret, E. Voutier, K. Wang, R. Wilson, B. Wojtsekhowski, and X. Zheng. Parity-violating electron scattering from ^{4}He and the strange electric form factor of the nucleon. *Phys. Rev. Lett.*, 96:022003, Jan 2006.

[8] D. Androic et al. First Determination of the Weak Charge of the Proton. 2013.

[9] Nuruzzaman. Q-weak: First direct measurement of the weak charge of the proton. *EPJ*, December 2013.

[10] C. W. Leemann, D. R. Douglas, and G. A. Krafft. "The Continuous Electron Beam Accelerator Facility: CEBAF at the Jefferson Laboratory". Annual review of nuclear and particle science, vol. 51, no. 1, pp. 413-450, 2001.

[11] 12 GeV Upgrade: Future Science at Jefferson Lab. http://www.jlab.org/12GeV/index.html.

[12] B. Poelker. Q-weak e-Source Issues. Q-weak Collaboration Meeting, Q-weak-DocDB1436: https://qweak.jlab.org/doc-private/ShowDocument?docid=1436, June 2011.

[13] C. Hernandez-Garcia, P. G. O'Shea, and M. L. Stutzman. *Electron sources for accelerators.* Physics Today, February 2008.

[14] J. Grames, P. Adderley, J. Benesch, J. Clark, J. Hansknecht, R. Kazimi, D. Machie, M. Poelker, M. Stutzman, R. Suleiman, and Y. Zhang. Two wien filter spin flipper. *Particle Accelerator Conference Proceedings*, page 862, 2011.

[15] Kathrine Myers. *The First Determination of the Proton's Weak Charge Through Parity-Violating Asymmetry Measurements in Elastic e+p and e+Al Scattering.* PhD thesis, The George Washington University, Washington, DC 20052, USA, May 2012.

[16] Nuruzzaman and *et. all.* List of Beam Components & Critical BPMs. Qweak-docdb-1203, Feb 2010.

[17] Sarah Phillips. *Measurement of the Strange Quark Contribution to the Vector Structure of the Proton.* PhD thesis, College of William and Mary, Virginia, Nov 2007.

[18] G. Krafft and A. Hofler. How the Linac Beam Position Monitors Work. CEBAF Technical Note CEBAF-TN-93-004, 1993.

[19] Andrew James Ruehe Puckett. *Recoil Polarization Measurements of the Proton Electromagnetic Form Factor Ratio to High Momentum Transfer.* PhD thesis, Massachusetts Institute of Technology, MA, Feb 2010.

[20] M. Hauger, A. Honegger, J. Jourdan, G. Kubon, T. Petitjean, D. Rohe, I. Sick, G. Warren, H. Whrle, J. Zhao, R. Ent, J. Mitchell, D. Crabb, A. Tobias, M. Zeier, and B. Zihlmann. A

high-precision polarimeter. *Nuclear Instruments and Methods in Physics Research Section A: Accelerators,Spectrometers,Detectors and Associated Equipment*, 462(3):382 – 392, 2001.

[21] Paul Gueye. Status of the actual beam position monitors in the Hall C beamline. CEBAF Technical Note Unpublished internal document, December 1995.

[22] Nuruzzaman and *et. all*. Position and Angle Determination at the Q^p_{weak} Target for Beam Modulation. Qweak-docdb-1208, March 2010. Used as a reference for how the position and angle determination at the target for beam modulation in the Q^p_{weak} experiment.

[23] Buddhini Waidyawansa. *A 3% Measurement of the Beam Normal Single Spin Asymmetry in Forward Angle Elastic Electron-Proton Scattering using the Qweak Setup*. PhD thesis, Ohio University, Athens OH 45701, USA, August 2013.

[24] Benjamin Micheal Patrick Clasie. *Measurement of Nuclear Transparency from $A(e,e'\pi^+)$ Reactions*. PhD thesis, Massachusetts Institute of Technology, MA, Aug 2006.

[25] Nuruzzaman. *Effective Kaon-Nucleon Cross Section from Nuclear Transparency Measured in the $A(ee'K^+)$ Reaction*. PhD thesis, Mississippi State University, MS, Aug 2010.

[26] Ramesh Subedi. Summary report on the BCMs for QWEAK. Qweak-docdb-1777, January 2013.

[27] Nuruzzaman and *et. all*. How Beam Energy will be Identified in Q^p_{weak}. Qweak-docdb-1149, January 2010. Used as a reference for how the beam enegy will be identified in the Q^p_{weak} experiment.

[28] C. Yan, R. Carlini, and D. Neuffer. Beam energy measurement using the Hall C beamline. *Conf.Proc.*, C930517:2136–2138, 1993.

[29] C. Yan, P. Adderley, D. Barker, J. Beaufait, K. Capek, R. Carlini, J. Dahlberg, E. Feldl, K. Jordan, B. Kross, W. Oren, R. Wojcik, and J. VanDyke. Superharp ? a wire scanner with absolute position readout for beam energy measurement at {CEBAF}. *Nuclear Instruments and Methods in Physics Research Section A: Accelerators, Spectrometers, Detectors and Associated Equipment*, 365(2?3):261 – 267, 1995.

[30] OPTIM: Computer code for linear and non-linear optics calculations. `http://www-bdnew.fnal.gov/pbar/organizationalchart/lebedev/OptiM/optim.htm`.

[31] Nuruzzaman and *et. all.* Beam Modulation in the 3C Line for the Q^p_{weak} Experiment. Hall-c technical note, Jun 2009. Beam Modulation write up for Q^p_{weak} experiment.

[32] Valery Lebedev. Computer code for linear and non-linear optics calculations. http://www-bdnew.fnal.gov/pbar/organizationalchart/lebedev/OptiM/optim.htm, Jun 2007.

[33] M. Hauger, A. Honegger, J. Jourdan, G. Kubon, T. Petitjean, D. Rohe, I. Sick, G. Warren, H. Whrle, J. Zhao, R. Ent, J. Mitchell, D. Crabb, A. Tobias, M. Zeier, and B. Zihlmann. A high-precision polarimeter. *Nuclear Instruments and Methods in Physics Research Section A: Accelerators, Spectrometers, Detectors and Associated Equipment*, 462(3):382 – 392, 2001.

[34] Matthias Loppacher. *Moller polarimeter for CEBAF Hall-C*. PhD thesis, University of Basel, Basel, April 1996.

[35] Rakitha Beminiwattha. *A Measurement of the Weak Charge of the Proton through Parity Violating Electron Scattering using the Qweak Apparatus: A 21% Result*. PhD thesis, Ohio University, Athens OH 45701, USA, August 2013.

[36] A. Narayan. Precision Compton Polarimetry During the Qweak Experiment. DNP 2012 Conference, Q-weak-DocDB1732: https://qweak.jlab.org/doc-private/ShowDocument?docid=1732, October 2012.

[37] Amrendra Narayan. *Electron Detector in Compton polarimeter for CEBAF Hall-C*. PhD thesis, Mississippi State University, Mississippi State, MS, April 2013.

[38] Juan Carlos Cornejo. *Photon Detector in Compton polarimeter for CEBAF Hall-C*. PhD thesis, College of William and Mary, Williamsburg, VA, USA, April 2014.

[39] Gregory Smith, Silviu Covrig, and Jim Dunne. "Qweak Liquid Hydrogen Target: Preliminary Design & Safety Document". Qweak-docdb-1041, August 2009.

[40] ANSYS: A fluid dynamics simulation code. http://www.ansys.com/.

[41] Gregory Smith. "Optics Target". Qweak-docdb-1144, December 2009.

[42] Juliette Mammei. *Parity-Violating Elastic Electron Nucleon Scattering: Measurement of the Strange Quark Content of the Nucleon and Towards a Measurement of the Weak Charge of the Proton*. PhD thesis, Virginia Polytechnic Institute & State University, Blacksburg, VA 24061-0002, USA, April 2010.

[43] Peiqing Wang. Magnetic Field Simulation and Mapping for the Q^p_{Weak} Experiment. Master's thesis, University of Manitoba, Winnipeg, Manitoba, Canada, 2009.

[44] Nuruzzaman. Hall Probe Mount Design for QTOR. Qweak-docdb-1244, May 2010.

[45] Peiqing Wang. Simulated elastic flux images on main bars. ELOG-Analysis-588: https://qweak.jlab.org/elog/Analysis+&+Simulation/588, May 2012.

[46] Peiqing Wang. *A Measurement Of The Protons Weak Charge Using An Integration Cerenkov Detector System*. PhD thesis, University of Manitoba, Winnipeg, Manitoba, Canada, June 2011.

[47] Jie Pan. *Towards a Precision Measurement of Parity-Violating e-p Elastic Scattering at Low Momentum Transfer*. PhD thesis, University of Manitoba, Winnipeg, Manitoba, Canada, June 2012.

[48] John Leacock. *Measuring the Weak Charge of the Proton and the Hadronic Parity Violation of the $N \to \Delta$ Transition*. PhD thesis, Virginia Polytechnic Institute & State University, Blacksburg, VA 24061-0002, USA, October 2012.